HHS Public Access

Author manuscript

Neuroscience. Author manuscript; available in PMC 2017 June 02.

Published in final edited form as:

Neuroscience. 2016 June 2; 324: 321–329. doi:10.1016/j.neuroscience.2016.02.074.

Ablation of fast-spiking interneurons in the dorsal striatum, recapitulating abnormalities seen post-mortem in Tourette syndrome, produces anxiety and elevated grooming

Meiyu Xu, Ph.D.[1,†], **Lina Li, BA**[1], and **Christopher Pittenger, MD, Ph.D.**[1,2,3,4,*]

[1]Department of Psychiatry, Yale University, New Haven, CT

[2]Department of Psychology, Yale University, New Haven, CT

[3]Child Study Center, Yale University, New Haven, CT

[4]Interdepartmental Neuroscience Program, Yale University, New Haven, CT

Abstract

Tic disorders, including Tourette syndrome (TS), are thought to involve pathology of cortico-basal ganglia loops, but their pathology is not well understood. Post-mortem studies have shown a reduced number of several populations of striatal interneurons, including the parvalbumin-expressing fast spiking interneurons (FSIs), in individuals with severe, refractory TS. We tested the causal role of this interneuronal deficit by recapitulating it in an otherwise normal adult mouse using a combination transgenic-viral cell ablation approach. FSIs were reduced bilaterally by ~40%, paralleling the deficit found post-mortem. This did not produce spontaneous stereotypies or tic-like movements, but there was increased stereotypic grooming after acute stress in two validated paradigms. Stereotypy after amphetamine, in contrast, was not elevated. FSI ablation also led to increased anxiety-like behavior in the elevated plus maze, but not to alterations in motor learning on the rotorod or to alterations in prepulse inhibition, a measure of sensorimotor gating. These findings indicate that a striatal FSI deficit can produce stress-triggered repetitive movements and anxiety. These repetitive movements may recapitulate aspects of the pathophysiology of tic disorders.

INTRODUCTION

Tic disorders affect 5% of the population and produce significant morbidity (Du et al., 2010). Gilles de la Tourette syndrome (TS), characterized by both vocal and motor tics, represents part of this continuum. Tics are commonly comorbid with other forms of neuropsychiatric pathology, including obsessive-compulsive disorder (OCD) and attention deficit disorder (ADHD); indeed, 90% of patients diagnosed with TS have at least one

*Correspondence: 34 Park Street, W315, New Haven, CT 06519, 203-974-7675, Christopher.pittenger@yale.edu.
†Current address: Brown University, Providence, RI

additional diagnosis (Du et al., 2010, Hirschtritt et al., 2015). Existing pharmacotherapies are of limited efficacy (Bloch, 2008). Tics fluctuate over time and are exacerbated by stress (Leckman, 2002, Du et al., 2010, Kurlan, 2010) and by acute psychostimulant challenge (Denys et al., 2013). Individuals with TS often have deficits in procedural learning (Marsh et al., 2004), sensorimotor gating (Swerdlow et al., 2001, Castellan Baldan et al., 2014), and fine motor control (Bloch et al., 2006), though these are not part of contemporary diagnostic criteria.

Convergent data implicate abnormalities of the basal ganglia-thalamo-cortical circuitry in TS (Leckman et al., 2010, Williams et al., 2013b), although it is increasingly clear that dysfunction in other brain circuitries is also implicated (Leckman et al., 2010, Neuner et al., 2013, Williams et al., 2013a). The striatum is the main input nucleus of the basal ganglia. Its principal cells, the medium spiny neurons (MSNs), receive glutamatergic input from cortex and thalamus and dopaminergic modulation from the substantia nigra. MSNs comprise >90% of the neurons in the rodent striatum; their activity is modulated by several different populations of interneuron.

Parvalbumin-expressing fast-spiking interneurons (FSIs) constitute about 1% of striatal neurons. PV interneurons integrate glutamatergic inputs from cortex and form strong GABAergic synapses on the somata of nearby MSNs, forming a potent feedforward inhibitory circuit (Mallet et al., 2005, Tepper et al., 2010). A single FSI can exert powerful inhibitory control on the activity of a large number of nearby MSNs (Koos and Tepper, 1999). This feed-forward inhibition is thought to have an important role in orchestrating striatal information processing (Berke, 2011). FSIs coordinate MSN firing in the theta-band range in certain behavioral states (Berke et al., 2004) and fire in concert during action selection (Gage et al., 2010).

Post-mortem examination of brains from individuals with a history of severe TS has revealed abnormalities in striatal FSIs (Kalanithi et al., 2005, Kataoka et al., 2010). However, such observations cannot elucidate the causal role of this deficit: whether it is causal, compensatory, epiphenomenal, or a consequence of years of treatment. Several lines of evidence suggest a casual role. Transient pharmacological inhibition of FSIs produces movement abnormalities (Gittis et al., 2011), but it is unclear what would happen with more chronic disruption of FSI activity, which is implied by the absence of these cells in post-mortem material. Reduced FSIs are also seen in the dt^{sz} dystonic hamster, a spontaneously occurring mutant with movement abnormalities (Gernert et al., 2000), and in the SAPAP3 knockout mouse, which exhibits elevated, repetitive grooming (Burguiere et al., 2013); but these deficits occur in the context of widespread abnormalities, some of which may be developmental, and thus their causal role in the development of abnormal behaviors is no more clear than it is patients.

We sought to more directly address the question of whether chronic disruption of striatal FSIs, in an otherwise normal brain, is sufficient to produce TS-relevant phenomenology. We have recently described a strategy for the targeted ablation of defined interneuronal populations (Xu et al., 2015a). This permits the temporally, spatially, and cell-type specific recapitulation of the neuropathological changes seen post-mortem in TS in an otherwise

normal adult brain. Here we applied this strategy to striatal FSIs and examined the consequences of their ablation.

Importantly, demonstration of a causal connection between a FSI deficit and behavioral pathology does not require recapitulation of all aspects of TS phenomenology. It is increasingly recognized that many neuropsychiatric diagnoses do not represent unitary natural kinds (Insel et al., 2010) and are causally heterogeneous, and that modeling trandiagnostic endophenotypes is a more realistic prospect than modeling diagnostic entities in all of their complexity (Nestler and Hyman, 2010). Striatal FSI deficiency has been associated with severe TS (Kalanithi et al., 2005, Kataoka et al., 2010), but it is not known whether this finding is specific to severe, treatment-refractory disease, to TS or tic disorders more generally, or to a range of behavioral pathology that extends beyond the boundaries of current diagnostic entities. We therefore tested a range of behaviors that capture different aspects of the symptomatology of TS and related disorders.

EXPERIMENTAL PROCEDURES

All experiments were performed in accordance with the NIH Guide for the Use of Laboratory Animals and were approved by the Yale University Institutional Animal Care and Use Committee. Mice were housed in a temperature and climate-controlled facility on a 12-hour light/dark schedule.

Vector constructs and AAV virus production

We engineered a recombinant adeno-associated virus that expresses eGFP (Heim et al., 1995) in infected cells in the absence of *Cre* recombinase but expresses the simian diphtheria toxin receptor (sDTR; Buch et al., 2005) in *Cre*-expressing cells, rendering them sensitive to ablation after systemic administration of diphtheria toxin (Xu et al., 2015a). EGFP and sDTR, in the antisense orientation and tagged with a FLAG epitope for ready immunodetection, are contained within a modified FLEX cassette, with eGFP between the lox p and lox 2722 sites at the 5′ end of the FLEX cassette. We have previously used the elongation factor 1a promoter to drive expression from the eGFP/sDTR cassette (Xu et al., 2015a); however, in pilot experiments we found sDTR expression from this promoter to be low in virus-infected striatal FSIs (data not shown), and we therefore replaced it with the more powerful CAG promoter (Miyazaki et al., 1989). To prevent excessive and potentially toxic eGFP expression in virus-infected *Cre*-negative cells, we introduced a stem-loop structure sequence (TACTGCTATACTAATAGGTATAGCAGTA) into the 5′ end of the eGFP mRNA, which reduces eGFP translation without affecting the sDTR mRNA in *Cre*-positive cells. The resulting vector is termed iDTR A46 (Figure 1A).

A negative control construct, C46, is identical to A46 except for multiple point mutations in the 3′ Lox sites, as in (Xu et al., 2015a). This prevents *Cre*-mediated inversion, such that infected cells always express eGFP (and not sDTR), irrespective of whether they express *Cre* (Figure 1A).

These constructs were packaged into AAV (rh10 serotype) by the Salk Institute viral vector core (vectorcore.salk.edu), with a titer of $1X10^{13}$ genomic copies per mL by real-time PCR.

rh10 provides superior spread in the striatum after a single injection without significant anterograde or retrograde infection (Cearley and Wolfe, 2006, Xu et al., 2015a).

In vivo viral infusion and virus validation

Adult male hemizygous PV-*Cre* transgenic mice were produced in our vivarium by crossing heterozygous male Pvalbm1(*Cre*)Arbr mice (www.jax.org:008069) with female wild type C57BL/6 breeders (Jackson Laboratories). Stereotaxic surgery was performed at age 3–4 months following standard procedures. PV-*Cre* mice were anesthetized with an intraperitoneal injection of xylazine (10 mg/kg, Bayer) and ketamine (100 mg/kg, Merial). A 2 μl Hamilton syringe attached to a micropump (UltramicroPump II; World Precision Instruments, Sarasota, FL, USA) was lowered through a skull burr hole into the striatum at the coordinates: AP + 0.8 mm; ML ± 2.3 mm; DV – 3.5 mm relative to bregma (Paxinos and Franklin, 2004). 0.5 μl of virus was infused bilaterally at a flow rate of 0.1 μl/min. The Hamilton syringe was left in place for 10 min after completion of the infusion, to eliminate back-flow, and then slowly withdrawn. This process was repeated on the other side. The scalp was then sutured; after recovery, mice were returned to their home cage for a minimum of two weeks post-surgery.

For validation experiments (Figure 1A–C), mice received A46 virus on one side and C46 contralaterally; for behavioral experiments (Figures 1D,E, 2–4), mice received either A46 or C46 bilaterally. Some mice in validation experiments were sacrificed 2 weeks later, without DT administration (Figure 1A). In all other experiments, mice were injected with DT (15 mg/kg intraperitoneal in sterile saline) once daily for 3 days; this dosing regimen was found in pilot experiments (not shown) to provide optimal FSI ablation.

Behavioral characterization took place over 6 weeks; mice were euthanized at 5–6 months. All brains were examined histologically after the completion of behavioral experiments; the extent of viral spread and PV-expressing neuron reduction were established using immunostaining. 8 animals in which viral delivery throughout the dorsal striatum was not achieved bilaterally or diffusion into the overlying cortex was substantial were excluded from behavioral experiments, prior to data analysis. The region of viral spread, after exclusions, is shown qualitatively in Figure 1D.

Elevated plus maze, rotorod, and prepulse inhibition

Elevated plus maze, prepulse inhibition and motor learning on the rotorod were tested as previously described (Castellan Baldan et al., 2014, Xu et al., 2015a). These tests were done prior to stressful tests, described below, and to amphetamine challenge, to reduce the risk of influence of one behavioral task on a subsequent one; all behavioral tests were separated by at least 1 week.

Startle-induced stress

Startle-induced stress and subsequent monitoring of spontaneous behaviors was performed as described previously (Xu et al., 2015a). Briefly, unpredictable presentation of a white noise acoustic startle stimulus was used as an acute mild stressor. This was performed in a prepulse inhibition chamber (San Diego Instruments, San Diego, CA), but with the door

open and the mice unrestrained in an open, clear-sided box. Mice were videotaped and visually monitored before, during, and for 30 minutes after this stressor. Time spent in repetitive behaviors, which consisted primarily of increased grooming, was scored for 10 minutes during each stage by an observer blind to experimental condition. Stereotyped grooming can be scored in more refined ways than we have attempted here; for example, Berridge and colleagues have described the complex topography of normal grooming and how it evolves into stereotypic chains under pathological conditions (Kalueff et al., 2016). It remains unclear, however, what aspect of rodent grooming or stereotypical behavior best recapitulates the mechanisms of human tics; we have therefore taken a conservative, theory-free approach and scored time spent in all grooming and other repetitive behaviors as a single measure.

Fear conditioning and fear-induced grooming

Fear-induced grooming was assayed as recently described (Xu et al., 2015b). Briefly, on day 1, mice underwent tone fear conditioning, following a standard protocol (30 s tone conditioned stimulus [CS], 2 s 0.4V footshock unconditioned stimulus [US]; 2 CS-US pairings separated by 90 s). 48 hour later mice were placed in a clear box and videotaped for 30 min before and 30 min after 30 sec presentation of the CS. Freezing was scored during the 30 sec CS presentation. Total time spent grooming was scored from videotape before and after CS presentation. Both freezing and grooming were scored by an observer blind to experimental condition.

Immunohistochemistry

Immunostaining for PV, ChAT and FLAG was performed following standard procedures (Xu et al., 2015a). For PV cell counting we used mouse anti-PV (P3088, Sigma, 1:2500) and biotinylated goat anti-mouse immunoglobulin secondary (Vector Laboratories: BA-9200, 1:500). For ChAT cell counting we used goat ant-ChAT primary antibody (Millipore: AB144P, 1:500) and biotinylated rabbit anti-goat immunoglobulin second antibody (Vector Laboratories: BA-5000, 1:1000). In both cases these were visualized using the Vectastain Elite ABC kit (Vector Laboratories) and diamionbenzidine substrate (Vector Laboratories).

Cell counting was performed using Stereoinvestigator (MBF Biosciences), as in our recent work (Xu et al, 2015a). 40 μm coronal slices were continuously collected throughout the forebrain and stored in cryoprotectant solution (30% glycerin, 30% ethylene glycol, 0.2 X PBS solution) at 4 °C. Slices through the dorsal striatum at 240 μm intervals were selected for staining. Staining was performed as in Xu et al, 2015a. After development with diaminobenzidine and mounting, coronal sections were selected on the basis of anatomical criteria to match A-P levels +1.18, 0.98, 0.74, 0.50, and 0.26 mm, relative to bregma, with reference to Paxinos and Franklin (2004). Because of the relatively small number of ChAT and PV interneurons in the striatum, we counted all visible immunostained cells in these sections. On each side of each section, the striatum was outlined using StereoInvestigator, again with reference to Paxinos and Franklin (2004). Stereoinvestigator was used to systematically examine all fields within this region; all stained cells were counted (using a stereological dissector to avoid over-counting). Total stained cells, bilaterally, were summed across the 5 sections specified above for each animal, and normalized to the total striatal

area across the five sections to ensure comparability cross mice. All values were normalized to the average cell density within the control group in each analysis for presentation.

For fluorescent staining, primary antibodies were mouse anti-FLAG (1:500; Sigma F1804), Chicken anti-GFP (1:2000; Abcam Ab13970), and rabbit anti-PV (ab11427, abcam) 1:1000. Second antibodies were Alexa fluor 594-conjugated goat anti-mouse (1:400; Life Technologies A11032), Alexa fluor 488-conjugated goat anti-chicken (1:400; Life Technologies A11039), and Alexa fluor 633-conjugated goat anti-rabbit (1:400; Life Technologies A21071). Confocal images were taken using a laser scanning confocal microscope (Olympus Fluoview FV300) at 200×.

Statistical analysis

Data were organized using Microsoft Excel and analyzed using SPSS (IBM). 2-tailed statistics were used for all comparisons. T-tests, repeated-measure ANOVA, and Mann-Whitney U tests were used, as appropriate and as described in the text.

RESULTS

Targeted ablation of PV-expressing interneurons in the adult mouse brain

We injected the dorsal striatum of adult male PV-*Cre* transgenic mice with virus iDTR-A46 on one side and the negative control virus iDTR-C46 contralaterally (Figure 1A; see Methods). Mice were injected with either DT (15 ng/g body weight intraperitoneal daily x 3 days) or saline two weeks after surgery and then sacrificed 1 week later. In saline-treated mice, eGFP expression was visible broadly throughout the striatum on both sides, demarcating viral spread; FLAG imunoreactivity, which reflects sDTR expression, was seen only in PV-immunoreactive cells (Figure 1B). FLAG expression was never seen on the C46-infected side.

Repetitive behaviors after PV interneuron ablation in the dorsal striatum

We characterized behavioral phenotypes that parallel TS symptoms in PV-ablated mice. PV-*Cre* mice received A46 or C46 virus bilaterally in the dorsal striatum (n = 10 A46, 8 C46, after exclusions for poor viral targeting). Two weeks later, all mice received DT, as before, followed one week later by behavioral analysis. Subsequent assessment of virus spread confirmed broad infection of the dorsal striatum (Figure 1D), with a statistically significant ~40% reduction in PV interneuron density (Fig. 1E; Mann-Whitney $U = 0$, $p < 0.0001$) in the dorsal striatum. To confirm the specificity of ablation we also immunostained cholinergic interneurons in this tissue. There was no reduction in ChAT-positive interneurons in A46 mice (Mann-Whitney $U = 18$, N.S.). If anything, the trend was towards a greater density of ChAT-positive cells in PV-ablated, though this did not reach statistical significance. There was no significant association between ChAT and PV cell density in either ablated ($F[1,8] = 1.3$, $p > 0.2$) or control animals ($F[1,6] = 1.129$, $p > 0.2$).

PV-ablated mice did not exhibit detectable repetitive behaviors at baseline (not shown). Clinically, tics fluctuate dramatically in TS; they are enhanced by stress, acute psychostimulant administration, and sleep deprivation (Leckman, 2002, Lin et al., 2007, Du

et al., 2010, Kurlan, 2010, Denys et al., 2013). To test the ability of acute stress to potentiate repetitive behaviors that might relate to tics, we used two acute stress protocols that we have recently described in other TS models (Xu et al., 2015a, Xu et al., 2015b).

We exposed FSI-ablated animals (and C46-injected controls) to 11 minutes of repeated unpredictable acoustic startle (Xu et al., 2015a). Grooming, stereotypy, and other behaviors were observationally scored from video before, during, and after this block of startle stimuli. PV-ablated mice exhibited no behavioral abnormalities prior to the stressor, but increased grooming during the 11-minute startle block and in the 30 minutes after the end of the startle stimuli (Figure 2A; Supplementary video; mixed ANOVA: group, $F [1,16]=9.439$, $p=0.007$; stage, $F [2,15]=12.713$, $p=0.001$; interaction, $F[2,15]=8.765$, $p=0.003$).

We next tested repetitive behaviors triggered by conditioned fear (Xu et al., 2015b). PV-ablated mice acquired tone fear conditioning, freezing normally when presented with the conditioned tone in a novel environment 48 hours after tone-shock pairing (Figure 2B; $t[16] = 0.476$, $p = 0.64$). During the 30 minutes following tone presentation, however, ablated mice exhibited increased grooming, recapitulating what we have seen in another TS model (Xu et al., 2015b). Because of the trend towards greater freezing in ablated animals, we included freezing as a covariate in the analysis of cue-induced grooming (Figure 2C; mixed ANCOVA: stage, $F[1,13]=16.805$, $p=0.001$; group, $F[1,13]=0.928$, $p=0.35$; interaction, $F[1,13]=5.275$, $p=0.039$).

In other TS models, including after ablation of cholinergic interneurons in the dorsolateral striatum, we have seen potentiated stereotypy after psychostimulant challenge (Castellan Baldan et al., 2014, Xu et al., 2015a). However, we found no difference between FSI-ablated and control mice after acute D-amphetamine challenge. Stereotypy and locomotor activity were scored from video using an automated system (HomeCageScan: Cleversys, Reston, VA). At 7 mg/kg D-amphetamine there was no difference in stereotypy (Figure 3A; RM-ANOVA: group, $F[1,16]=0.001$, $p=0.97$; time, $F[11,6]=6.867$, $p=0.014$; interaction, $F[11,6]=1.181$, $p=0.44$) or in locomotor activity (Figure 3B; group, $F[1,16]=0.124$, $p=0.729$; time, $F[11,6]=8.814$, $p=0.007$; interaction, $F[11,6]=0.489$, $p=0.856$). In a repeated experiment at 6 mg/kg D-amphetamine there was similarly no difference in stereotypy (Figure 3C; group, $F[1,13]=0.233$, $p>0.637$; time, $F[11,3]=1.066$, $p=0.545$; interaction, $F[11,3]=0.896$, $p>0.616$) or in locomotor activity (Figure 3D; group, $F[1,13]=0.101$, $p>0.756$; time, $F[11,3]=42.875$, $p=0.005$; interaction, $F[11,3]=7.383$, $p>0.063$). Because automated scoring may not be optimally sensitive for detecting stereotypies (Xu et al., 2015a), we manual re-scored in the latter experiment from video and again found no effect of FSI ablation (Figure 3E; group, $F[1,13]=1.684$, $p>0.217$; time, $F[11,3]=815$, $p<0.001$; interaction, $F[11,3]=2.186$, $p>0.283$).

Other behavioral tests

FSI-ablated mice showed higher anxiety-like behavior in the elevated plus maze (Figure 4A, B. Open arm time: Mann-Whitney U test, $p=0.012$; Open arm entries: Mann-Whitney U test, $p=0.083$), but normal total exploratory activity (Figure 4C; Mann-Whitney U test, $p=0.20$; normal exploratory activity is also apparent in Figure 3B, D prior to amphetamine administration). PV ablated mice were indistinguishable from controls in baseline

performance and motor learning on the rotorod (Figure D; RM-ANOVA: trial, F [5,12]=7.818, p=0.002; group, F [1,16]=0.037, p=0.85; interaction, F [5,12]=1.555, p=0.245).

There was no effect of FSI ablation on baseline startle magnitude (Figure 4E; t[16] = 0.462, p = 0.65), and no statistically significant effect on prepulse inhibition of startle (Figure 4F; RM-ANOVA: group, F[1,16] = 0.002, p = 0.968; prepulse intensity, F[2,15]=7.586, p=0.005; interaction, F[2,15]=3.325, p=0.064). The interaction term did approach significance, and a nominal effect of group was seen at the intermediate prepulse inhibition; it therefore remains possible that there is a subtle effect of FSI ablation on PPI.

DISCUSSION

These results establish the sufficiency of PV interneuron disruption in the dorsal striatum, which as has been documented in severe TS (Kalanithi et al., 2005, Kataoka et al., 2010), to produce repetitive grooming – after two different acute stressors. This suggests that the interneuronal deficit observed in patients is causally related to tics and other movement abnormalities, and not a compensatory change, an epiphenomenon, or a consequence of treatment. Our manipulation is unlikely to precisely recapitulate all pathological abnormalities in the TS brain; for example, deficits in other striatal interneurons have been documented (Kalanithi et al., 2005, Kataoka et al., 2010, Lennington et al., 2014). Furthermore, the deficit in PV interneurons may arise early during development in TS, and compensatory changes are to be expected; these may not be captured in our model. Disruption of interneurons early in development might produce different effects. We sought to capture a discrete and well-defined brain lesion, to ascertain whether and how it contributes to TS-relevant effects. In human disease a PV interneuronal deficit is likely to interact with other pathophysiological changes to produce the full clinical picture.

Modeling neuropsychiatric symptoms, including tics, in an animal model raises interpretive challenges (Nestler and Hyman, 2010, Pittenger, 2014). The behavioral abnormalities documented here differ from the tics that define TS. Simple tics are spasmodic, semi-voluntary movements of discrete groups of muscles that are typically unilateral and are most commonly seen in the face. Elevated grooming, on the other hand, represents enhancement of a normal behavioral pattern and is symmetrical. Elevated grooming, similar to what we have documented here, is seen in another mouse model of TS, with strong construct validity (Castellan Baldan et al., 2014, Xu et al., 2015a). On the other hand, grooming phenotypes have also been described in models that purport to recapitulate pathophysiology of OCD (Welch et al., 2007) and autism (Peca et al., 2011). Thus, while our findings are consistent with the proposal that interneuronal pathology in the dorsal striatum can predispose to neuropsychiatric symptomatology, including tics, they do not establish this abnormality as being specific to the TS or to the production of tics. Indeed, the abnormal movements produced by more acute inhibition of these cells have been described as resembling dystonia, rather than tics (Gittis et al., 2011). Clarifying the precise relationship between grooming phenotypes as a general marker of pathological change in animal models and the specific neuropsychiatric symptomatology seen in defined human conditions will require a much more detailed understanding of the pathogenic mechanisms seen in both systems.

The topography of grooming and related stereotypic behaviors can be analyzed in more detail than we have attempted here (Kalueff et al., 2016), and if the specific repetitive behaviors that are most isomorphic to human tics were clearly delineated and more specifically quantified, our behavioral scoring might be more sensitive to disease-relevant abnormalities. However, it is not clear which mouse behaviors represent the best model of tics; indeed, this may vary depending on various experimental or contextual factors, such as mouse strain. We have therefore taken an agnostic view and scored all repetitive behaviors as a single measure.

We observe these stereotypies only after stress challenge, not at baseline; this differs from what is seen in patients but is similar to the phenotype observed in a two other recently described TS models (Castellan Baldan et al., 2014, Xu et al., 2015a, Xu et al., 2015b). This may be simply a matter of assay sensitivity; quantification of tics or stereotypy, whether automated or manual, is of limited sensitivity and may miss low-amplitude movements. Alternatively, it may be that PV deficiency destabilizes the corticostriatal system, but not enough to produce spontaneous abnormal movements. More than one such pathophysiological 'hit,' such as pathology in other populations of interneuron (Kataoka et al., 2010, Lennington et al., 2014), may be required for spontaneous tic-like movements to emerge.

The consequences of PV ablation overlap with those we have recently documented after ablation of cholinergic interneurons (CINs) in the dorsolateral striatum (Xu et al., 2015a), but they also diverge in interesting ways. Stimulant-induced stereotypy was potentiated after CIN ablation (Xu et al., 2015a) but not after FSI ablation (Figure 3). This is intriguing in light of the well-established functional interactions between CINs and dopamine (e.g. Threlfell and Cragg, 2011, Threlfell et al., 2012); FSIs are not known to regulate DA. To the extent that the pathophysiological consequences for striatal function of CIN and FSI ablation converge, the effects of FSI ablation may be causally 'downstream' of dysregulation of DA. Interestingly, qualitatively different spontaneous movements are observed in conjunction with cholinergic interneuornal deficits in another recently-describd model, as a consequence of forebrain-wide deletion of the gene *torsinA* (Pappas et al., 2015). Further studies are needed to determine the precise relationship between different types of striatal abnormality and different categories of dystonic, tic-like, and repetitive movement.

On the other hand, FSI ablation produces anxiety-like behavioral abnormalities in the elevated plus maze (Figure 4A–C); this was not seen after CIN ablation (Xu et al., 2015a). Anxiety is not a primary symptom of TS, as currently defined (Leckman, 2002, Kurlan, 2010), but anxiety disorders and obsessive-compulsive disorder are commonly comorbid (Hirschtritt et al., 2015). Interestingly, SAPAP3 mutant mice, which exhibit a grooming phenotype and have been described as a model of OCD, also exhibit anxiety (Welch et al., 2007) and have recently been reported to have a deficit in striatal FSIs (Burguiere et al., 2013). These observations emphasize that the network and behavioral consequences of specific disease-associated pathophysiological abnormalities, such as deficits in striatal interneurons, may cut across traditional diagnostic categories.

These experiments have several limitations, to be addressed in future work. As noted above, we studied the consequences of PV interneuron ablation in adults; similar disruption early during development might have distinct consequence. We studied only male mice; TS has a male preponderance, but tics are also seen in females, and possible interactions of sex with pathophysiological mechanism cannot be examined in this study. We are, by design, recapitulating only one aspect of the putative pathophysiological abnormalities documented in post-mortem studies; the full clinical picture of TS is likely to arise from an interaction of PV interneuronal pathology with other processes.

This work highlights the importance of FSI dysregulation in the basal ganglia to the pathophysiology of TS. Our results suggest that the abnormalities seen *post mortem* (Kalanithi et al., 2005, Kataoka et al., 2010) represent a causal contributor to the pathophysiology of the disease, rather than a compensation, an epiphenomenon, or a consequences of pharmacological treatment.

Supplementary Material

Refer to Web version on PubMed Central for supplementary material.

Acknowledgments

The authors gratefully acknowledge Stacey Wilber and Jessica André for assistance with mouse colony maintenance and genotyping and Flora Vaccarino, Mounira Banasr, Marina Picciotto, and Ralph DiLeone for invaluable discussions during the development of the iDTR ablation system. This work has been supported by NIH grants R01MH091861 (CP) and K08MH081190 (CP), the Tourette Syndrome Association (CP, MX), the Allison Family Foundation (CP), and the State of Connecticut through its support of the Ribicoff Research Facilities at the Connecticut Mental Health Center.

References

Berke JD. Functional properties of striatal fast-spiking interneurons. Frontiers in systems neuroscience. 2011; 5:45. [PubMed: 21743805]

Berke JD, Okatan M, Skurski J, Eichenbaum HB. Oscillatory entrainment of striatal neurons in freely moving rats. Neuron. 2004; 43:883–896. [PubMed: 15363398]

Bloch MH. Emerging treatments for Tourette's disorder. Curr Psychiatry Rep. 2008; 10:323–330. [PubMed: 18627671]

Bloch MH, Sukhodolsky DG, Leckman JF, Schultz RT. Fine-motor skill deficits in childhood predict adulthood tic severity and global psychosocial functioning in Tourette's syndrome. Journal of child psychology and psychiatry, and allied disciplines. 2006; 47:551–559.

Buch T, Heppner FL, Tertilt C, Heinen TJ, Kremer M, Wunderlich FT, Jung S, Waisman A. A Cre-inducible diphtheria toxin receptor mediates cell lineage ablation after toxin administration. Nature methods. 2005; 2:419–426. [PubMed: 15908920]

Burguiere E, Monteiro P, Feng G, Graybiel AM. Optogenetic stimulation of lateral orbitofronto-striatal pathway suppresses compulsive behaviors. Science. 2013; 340:1243–1246. [PubMed: 23744950]

Castellan Baldan L, Williams KA, Gallezot JD, Pogorelov V, Rapanelli M, Crowley M, Anderson GM, Loring E, Gorczyca R, Billingslea E, Wasylink S, Panza KE, Ercan-Sencicek AG, Krusong K, Leventhal BL, Ohtsu H, Bloch MH, Hughes ZA, Krystal JH, Mayes L, de Araujo I, Ding YS, State MW, Pittenger C. Histidine decarboxylase deficiency causes Tourette syndrome: parallel findings in humans and mice. Neuron. 2014; 81:77–90. [PubMed: 24411733]

Cearley CN, Wolfe JH. Transduction characteristics of adeno-associated virus vectors expressing cap serotypes 7, 8, 9, and Rh10 in the mouse brain. Molecular therapy: the journal of the American Society of Gene Therapy. 2006; 13:528–537. [PubMed: 16413228]

Denys D, de Vries F, Cath D, Figee M, Vulink N, Veltman DJ, van der Doef TF, Boellaard R, Westenberg H, van Balkom A, Lammertsma AA, van Berckel BN. Dopaminergic activity in Tourette syndrome and obsessive-compulsive disorder. European neuropsychopharmacology: the journal of the European College of Neuropsychopharmacology. 2013; 23:1423–1431. [PubMed: 23876376]

Du JC, Chiu TF, Lee KM, Wu HL, Yang YC, Hsu SY, Sun CS, Hwang B, Leckman JF. Tourette syndrome in children: an updated review. Pediatrics and neonatology. 2010; 51:255–264. [PubMed: 20951354]

Gage GJ, Stoetzner CR, Wiltschko AB, Berke JD. Selective activation of striatal fast-spiking interneurons during choice execution. Neuron. 2010; 67:466–479. [PubMed: 20696383]

Gernert M, Hamann M, Bennay M, Loscher W, Richter A. Deficit of striatal parvalbumin-reactive GABAergic interneurons and decreased basal ganglia output in a genetic rodent model of idiopathic paroxysmal dystonia. J Neurosci. 2000; 20:7052–7058. [PubMed: 10995851]

Gittis AH, Leventhal DK, Fensterheim BA, Pettibone JR, Berke JD, Kreitzer AC. Selective inhibition of striatal fast-spiking interneurons causes dyskinesias. The Journal of neuroscience: the official journal of the Society for Neuroscience. 2011; 31:15727–15731. [PubMed: 22049415]

Heim R, Cubitt AB, Tsien RY. Improved green fluorescence. Nature. 1995; 373:663–664. [PubMed: 7854443]

Hirschtritt ME, Lee PC, Pauls DL, Dion Y, Grados MA, Illmann C, King RA, Sandor P, McMahon WM, Lyon GJ, Cath DC, Kurlan R, Robertson MM, Osiecki L, Scharf JM, Mathews CA. Tourette Syndrome Association International Consortium for G. Lifetime prevalence, age of risk, and genetic relationships of comorbid psychiatric disorders in tourette syndrome. JAMA psychiatry. 2015; 72:325–333. [PubMed: 25671412]

Insel T, Cuthbert B, Garvey M, Heinssen R, Pine DS, Quinn K, Sanislow C, Wang P. Research domain criteria (RDoC): toward a new classification framework for research on mental disorders. Am J Psychiatry. 2010; 167:748–751. [PubMed: 20595427]

Kalanithi PS, Zheng W, Kataoka Y, DiFiglia M, Grantz H, Saper CB, Schwartz ML, Leckman JF, Vaccarino FM. Altered parvalbumin-positive neuron distribution in basal ganglia of individuals with Tourette syndrome. Proceedings of the National Academy of Sciences of the United States of America. 2005; 102:13307–13312. [PubMed: 16131542]

Kalueff AV, Stewart AM, Song C, Berridge KC, Graybiel AM, Fentress JC. Neurobiology of rodent self-grooming and its value for translational neuroscience. Nature reviews Neuroscience. 2016; 17:45–59.

Kataoka Y, Kalanithi PS, Grantz H, Schwartz ML, Saper C, Leckman JF, Vaccarino FM. Decreased number of parvalbumin and cholinergic interneurons in the striatum of individuals with Tourette syndrome. The Journal of comparative neurology. 2010; 518:277–291. [PubMed: 19941350]

Koos T, Tepper JM. Inhibitory control of neostriatal projection neurons by GABAergic interneurons. Nat Neurosci. 1999; 2:467–472. [PubMed: 10321252]

Kurlan R. Clinical practice. Tourette's Syndrome. N Engl J Med. 2010; 363:2332–2338. [PubMed: 21142535]

Leckman JF. Tourette's syndrome. Lancet. 2002; 360:1577–1586. [PubMed: 12443611]

Leckman JF, Bloch MH, Smith ME, Larabi D, Hampson M. Neurobiological substrates of Tourette's disorder. Journal of child and adolescent psychopharmacology. 2010; 20:237–247. [PubMed: 20807062]

Lennington JB, Coppola G, Kataoka-Sasaki Y, Fernandez TV, Palejev D, Li Y, Huttner A, Pletikos M, Sestan N, Leckman JF, Vaccarino FM. Transcriptome Analysis of the Human Striatum in Tourette Syndrome. Biological psychiatry. 2014

Lin H, Katsovich L, Ghebremichael M, Findley DB, Grantz H, Lombroso PJ, King RA, Zhang H, Leckman JF. Psychosocial stress predicts future symptom severities in children and adolescents with Tourette syndrome and/or obsessive-compulsive disorder. Journal of child psychology and psychiatry, and allied disciplines. 2007; 48:157–166.

Mallet N, Le Moine C, Charpier S, Gonon F. Feedforward inhibition of projection neurons by fast-spiking GABA interneurons in the rat striatum in vivo. J Neurosci. 2005; 25:3857–3869. [PubMed: 15829638]

Marsh R, Alexander GM, Packard MG, Zhu H, Wingard JC, Quackenbush G, Peterson BS. Habit learning in Tourette syndrome: a translational neuroscience approach to a developmental psychopathology. Arch Gen Psychiatry. 2004; 61:1259–1268. [PubMed: 15583117]

Miyazaki J, Takaki S, Araki K, Tashiro F, Tominaga A, Takatsu K, Yamamura K. Expression vector system based on the chicken beta-actin promoter directs efficient production of interleukin-5. Gene. 1989; 79:269–277. [PubMed: 2551778]

Nestler EJ, Hyman SE. Animal models of neuropsychiatric disorders. Nat Neurosci. 2010; 13:1161–1169. [PubMed: 20877280]

Neuner I, Schneider F, Shah NJ. Functional neuroanatomy of tics. International review of neurobiology. 2013; 112:35–71. [PubMed: 24295617]

Pappas SS, Darr K, Holley SM, Cepeda C, Mabrouk OS, Wong JM, LeWitt TM, Paudel R, Houlden H, Kennedy RT, Levine MS, Dauer WT. Forebrain deletion of the dystonia protein torsinA causes dystonic-like movements and loss of striatal cholinergic neurons. eLife. 2015; 4:e08352. [PubMed: 26052670]

Paxinos, G.; Franklin, KBJ. The mouse brain in stereotaxic coordinates. Amsterdam; Boston: Elsevier Academic Press; 2004.

Peca J, Feliciano C, Ting JT, Wang W, Wells MF, Venkatraman TN, Lascola CD, Fu Z, Feng G. Shank3 mutant mice display autistic-like behaviours and striatal dysfunction. Nature. 2011; 472:437–442. [PubMed: 21423165]

Pittenger, C. Animal models of Tourette syndrome and obsessive-compulsive disorder. In: LeDoux, M., editor. Animal Models of Movement Disorders. San Deigo: Elsevier: Academic Press; 2014. p. 748-766.

Swerdlow NR, Karban B, Ploum Y, Sharp R, Geyer MA, Eastvold A. Tactile prepuff inhibition of startle in children with Tourette's syndrome: in search of an "fMRI-friendly" startle paradigm. Biological psychiatry. 2001; 50:578–585. [PubMed: 11690592]

Tepper JM, Tecuapetla F, Koos T, Ibanez-Sandoval O. Heterogeneity and diversity of striatal GABAergic interneurons. Frontiers in neuroanatomy. 2010; 4:150. [PubMed: 21228905]

Threlfell S, Cragg SJ. Dopamine signaling in dorsal versus ventral striatum: the dynamic role of cholinergic interneurons. Frontiers in systems neuroscience. 2011; 5:11. [PubMed: 21427783]

Threlfell S, Lalic T, Platt NJ, Jennings KA, Deisseroth K, Cragg SJ. Striatal dopamine release is triggered by synchronized activity in cholinergic interneurons. Neuron. 2012; 75:58–64. [PubMed: 22794260]

Welch JM, Lu J, Rodriguiz RM, Trotta NC, Peca J, Ding JD, Feliciano C, Chen M, Adams JP, Luo J, Dudek SM, Weinberg RJ, Calakos N, Wetsel WC, Feng G. Cortico-striatal synaptic defects and OCD-like behaviours in Sapap3-mutant mice. Nature. 2007; 448:894–900. [PubMed: 17713528]

Williams, K.; Bloch, MH.; State, MW.; Pittenger, C. Tourette syndrome. In: DSC, et al., editors. Neurobiology of Mental Illness. 4. New York: Oxford University Press; 2013a.

Williams, K.; Bloch, MH.; State, MW.; Pittenger, C. Tourette syndrome and tic disorders. In: Charney, DS., et al., editors. Neurobiology of Mental Illness. 4. New York: Oxford; 2013b.

Xu M, Kobets A, Du JC, Lennington J, Li L, Banasr M, Duman RS, Vaccarino FM, DiLeone RJ, Pittenger C. Targeted ablation of cholinergic interneurons in the dorsolateral striatum produces behavioral manifestations of Tourette syndrome. Proc Natl Acad Sci U S A. 2015a; 112:893–898. [PubMed: 25561540]

Xu M, Li L, Ohtsu H, Pittenger C. Histidine decarboxylase knockout mice, a genetic model of Tourette syndrome, show repetitive grooming after induced fear. Neurosci Lett. 2015b; 595:50–53. [PubMed: 25841792]

HIGHLIGHTS

- Tourette syndrome is associated with reduced interneurons in the striatum.
- We performed targeted ablation of parvalbumin neurons in the striatum in adult mice.
- Interneuronal ablation produced increased grooming after acute stress.
- Interneuronal ablation also produced elevated anxiety-like behavior.
- This supports a causal contribution of interneuronal deficits to movement disorders.

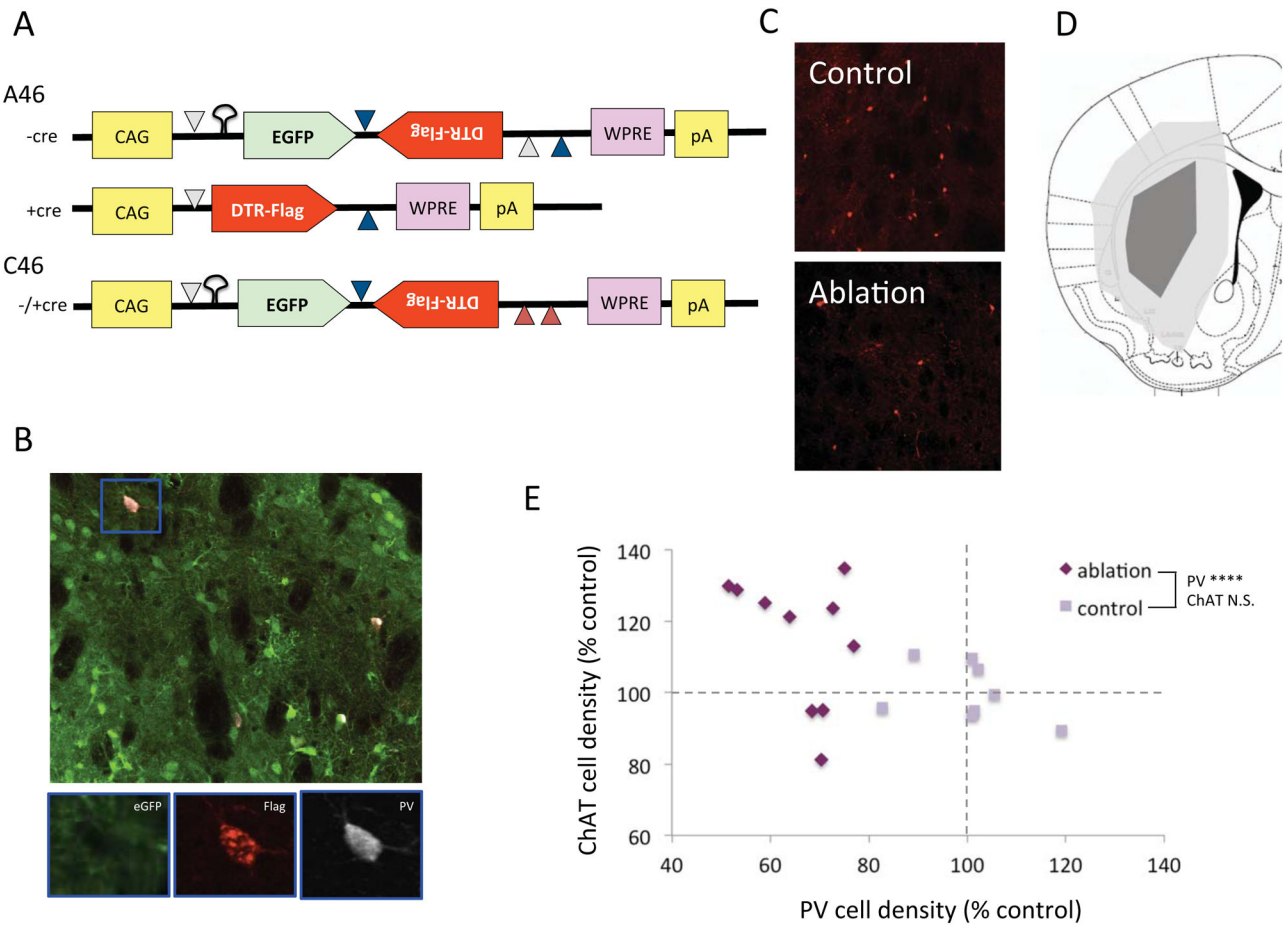

Figure 1. Targeted interneuronal ablation in the PV-*cre* mouse striatum

(**A**) Structure of the iDTR virus A46 and negative control virus C46. Recombination in the presence of CRE recombinase is mediated by matching *lox* elements, indicated as colored triangles; mutated 3′ *lox* elements in the C46 construct (red triangles) prevent recombination. CAG – synthetic promoter; eGFP – enhanced green fluorescent protein; DTR-Flag – Flag epitope-tagged simian diphtheria toxin receptor; WPRE – woodchuck hepatitis virus posttranscriptional regulator element; pA – poly-A mRNA cap. **B.** Triple immunostaining of striatal neurons after A46 virus infusion shows eGFP (green), FLAG (red) and PV (white); FLAG immunoreactivity, which corresponds to DTR expression, colocalizes specifically with PV. **C.** Reduced PV-expressing interneurons in the A46-injection dorsal striatum after systemic DT, as compared to contralateral control C46 virus. **D.** Spread of injected A46 virus in the dorsal striatum in mice used for subsequent behavioral experiments. **E.** PV-positive cell density was reduced ~40% in these animals, compared with C46-injected, DTR-treated PV-cre+ controls. ChAT-positive cells were not reduced in A46 virus-treated animals, supporting the specificity of the targeted ablation of PV-positive interneurons. Mann-Whitney U test (see Results): **** $p < 0.0001$ A46 vs C46 control group.

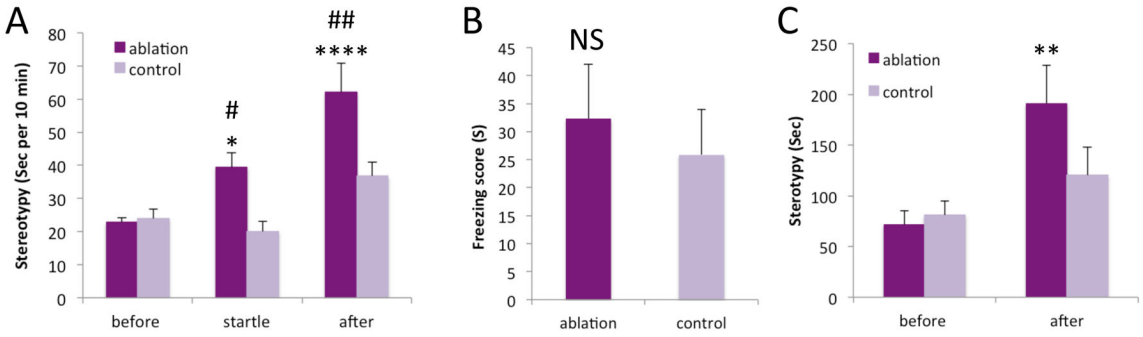

Figure 2. Stereotypy after FSI ablation

A. Grooming was elevated during and after acoustic startle stress in FSI-ablated mice. **B.** Freezing 48 hours after tone fear conditioning was normal in FSI-ablated mice. ∫**C.** Grooming was elevated after induction of conditioned fear in FSI-ablated mice. See text for statistics. Tukey's post-hoc: vs. same group baseline: * $p < 0.05$, ** $p < 0.01$, **** $p < 0.0001$; vs. control group same condition: # $p < 0.05$, ## $p < 0.01$.

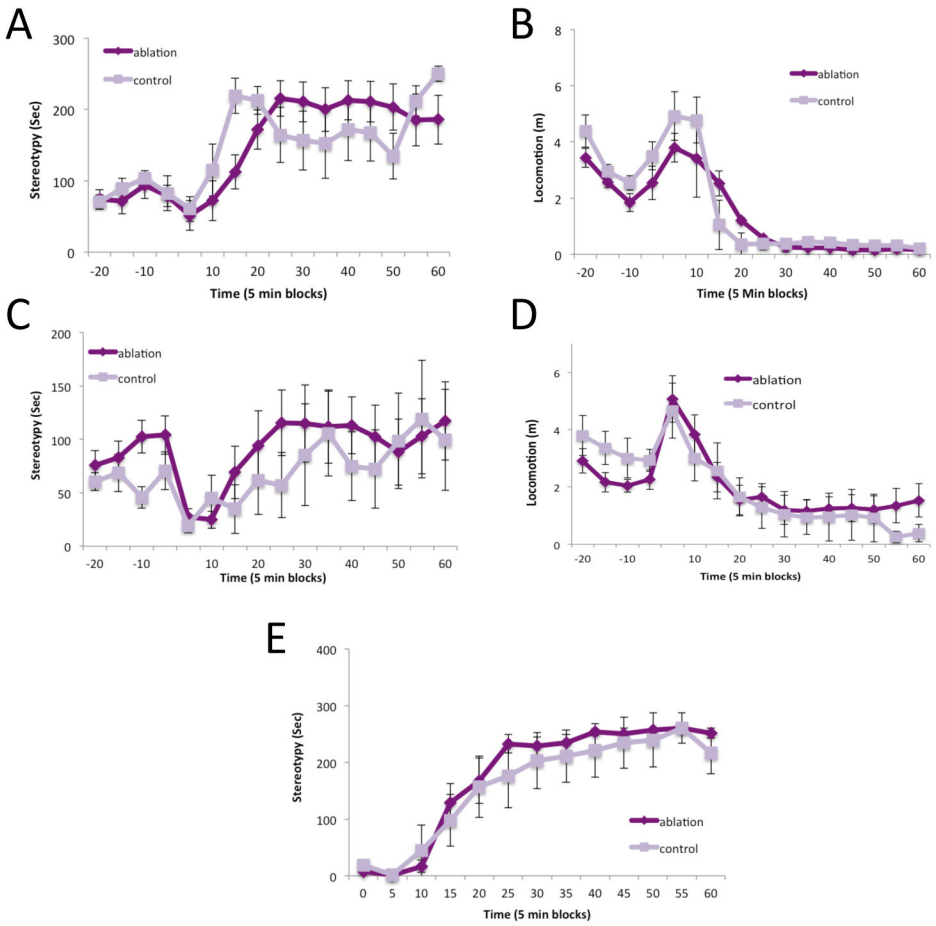

Figure 3. Normal stereotypy and locomotor activation after D-amphetamine in FSI-ablated mice

A. Stereotypy, scored from video using an automated system, after 7 mg/kg D-amphetamine; there was no effect of FSI ablation. **B.** Normal locomotor activation after 7 mg/kg D-amphetamine. **C.** Similarly, stereotypy was unchanged in FSI-ablated mice after 6 mg/kg D-amphetamine. **D.** Normal locomotor activation after 6 mg/kg D-amphetamine. **E.** Unchanged stereotypies after 6 mg/kg D-amphetamine were confirmed using manual scoring. See text for statistical analysis.

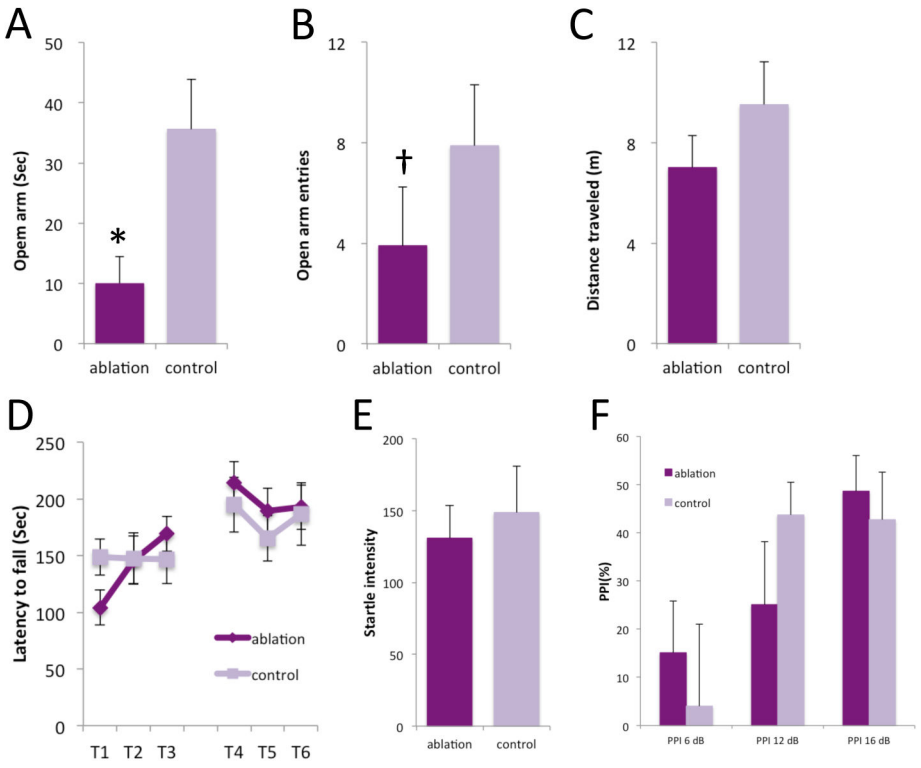

Figure 4. Motor behavior and anxiety after PV ablation

A–C. Several measures indicated increased anxiety in the elevated plus maze after FSI ablation. **D.** Exploratory activity was unaltered by FSI ablation in the elevated plus maze. **E.** Basal coordination and motor learning on the rotorod were unchanged after FSI ablation. **F.** Startle magnitude was not altered by striatal FSI ablation. **G.** Prepulse inhibition was not altered by striatal FSI ablation. See text for statistical analysis. * $p < 0.05$; † $p < 0.1$.